JOURNAL OF GEOPHYSICAL RESEARCH, VOL. 100, NO. C12, PAGES 24,691–24,703, DECEMBER 15, 1995

Solar heating of the Arctic mixed layer

G. A. Maykut
Department of Atmospheric Sciences, University of Washington, Seattle

Miles G. McPhee
McPhee Research Company, Naches, Washington

Abstract. Data from the 1975 Arctic Ice Dynamics Joint Experiment (AIDJEX) are used to examine energy exchange between the Arctic mixed layer and the ice pack. Conductivity-temperature-depth profiles from four drifting stations reveal significant heat storage in the upper 50 m of the water column during summer, with mixed layer temperature elevation above freezing δT reaching as high as 0.4°C. Combining δT with turbulent friction velocity obtained from local ice motion provides an estimate of heat flux from the ocean to the ice F_w which was found to be strongly seasonal, with maximum values reaching 40–60 W m^{-2} in August. The annual average value of F_w was 5.1 W m^{-2}, about half again as large as oceanic heat flux inferred from bottom ablation measurements in undeformed ice at the central station. Solar heat input to the upper ocean through open leads and thin ice, estimated using an ice thickness distribution model, totaled about 150 MJ m^{-2}, in general agreement with integrated values of F_w. Results indicate that oceanic heat flux to the ice in the central Arctic is derived mainly from shortwave radiation entering the ocean through the ice pack, rather than from diffusion of warm water from below. Indeed, during the AIDJEX project the mixed layer appears to have contributed 15–20 MJ m^{-2} of heat to the upper pycnocline. During the summer, F_w was found to vary by as much as 10–30 W m^{-2} over separations of 100 to 200 km and thus represents an important term in the surface heat budget not controlled by purely local deformation and thermodynamics.

1. Introduction

Model simulations by *Maykut and Untersteiner* [1971] demonstrated that the growth and overall thickness of sea ice is sensitive to the flux of sensible heat F_w released from the ocean at the underside of the ice. To reproduce the observed thickness of perennial ice in the Arctic Basin, their calculations required that undeformed ice receive an annual average F_w of about 2 W m^{-2}. Since this figure coincided roughly with estimates of heat loss in the central Arctic from the relatively warm Atlantic water that enters the basin through Fram Strait [*Crary*, 1960; *Panov and Shpaikher*, 1964], it was often assumed that upward diffusion into the mixed layer from below was the source of oceanic heat at the surface. However, the presence of a cold halocline between the mixed layer and deeper warm water makes it unlikely that much of the heat lost by the Atlantic layer can reach the ice pack directly [*Coachman and Barnes*, 1962]. Salinity and temperature data indicate that this halocline is maintained by lateral advection of cold dense water generated on the shelves and that it acts as a heat sink for the underlying Atlantic water [*Aagaard et al.*, 1981]. Thus, unlike the Southern Ocean and Fram Strait region where there are sizable contributions to F_w from the deeper ocean, the Arctic mixed layer is, to a large extent, thermodynamically decoupled from the deeper water. This means that a different source of energy is needed to explain F_w values in most parts of the Arctic Basin.

Paper number 95JC02554.
0148-0227/95/95JC-02554$05.00

An obvious energy source is shortwave radiation F_r entering the mixed layer through leads and thin ice during the spring and summer. Using ice strain observations and climatological data on F_r, *Maykut* [1982] calculated daily ice concentrations throughout the year in the Beaufort Sea and estimated that the amount of shortwave energy absorbed below the bottom of the ice pack was of the order of 100 MJ m^{-2} yr^{-1} (an annual average of about 3.2 W m^{-2}), more than enough to provide the F_w needed by undeformed ice. Excess energy, it was argued, would go to more rapid melting of deformed ice. If F_w is derived from shortwave radiation, the regional heat and mass balance of the ice pack will be strongly influenced by the amount of open water present during periods when F_r is large, i.e., by the degree of dynamic activity and by the amount of thinner ice present at the onset of the melt season. In addition, it is reasonable to expect that F_w would be strongly time-dependent, rather than constant throughout the year.

The origin, magnitude, and variability of F_w are of particular concern in climate models and coupled global circulation models that include the polar oceans. Intuitively, we might expect the system to behave as an "ice bath," with energy absorbed in the water being lost almost instantaneously to the ice through lateral and bottom melting. This has been a tacit assumption in most ice modeling and was consistent with turbulence models that treated the flux of heat and salt as analogous to momentum flux [*Josberger*, 1983; *Mellor et al.*, 1986], resulting in very efficient transfer whenever the ice was in motion relative to the underlying water. However, the ice-bath paradigm ignored observations that an ice-covered mixed layer could store heat (i.e., remain above freezing) for extended times [*McPhee*, 1986; *Perovich and Maykut*, 1990], a point discussed in the context of

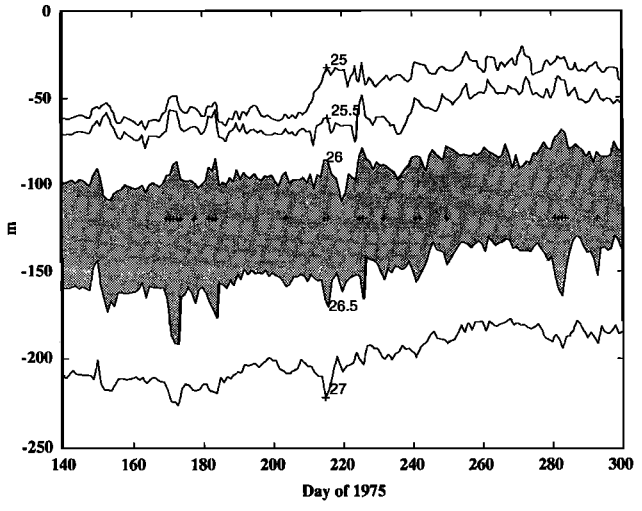

Figure 1. Contours of σ_0 (equal to $\rho_0 - 1000$ kg m^{-3}, where ρ_0 is density at surface pressure) at station Blue Fox. The separation between $\sigma_0 = 26$ and 26.5 kg m^{-3} (shown by the stippled region) was used to identify anticyclonic eddies, which are marked by pluses and were not used in the heat flux and budget calculations.

modeling the marginal ice zone by *Røed* [1984]. Also, the first direct measurements of turbulent heat flux in the ice/ocean boundary layer during the 1984 Marginal Ice Zone Experiment (MIZEX) demonstrated that F_w was dominated by molecular effects in thin sublayers near the ice-water interface that had no direct counterpart in the momentum flux process [*McPhee et al.*, 1987]. This was consistent with laboratory studies of heat transfer over hydraulically rough surfaces [*Yaglom and Kader*, 1974]. The MIZEX work was later combined with data from other Arctic projects to show that despite large differences in the apparent roughness of the ice underside (equivalent to large variation in drag coefficient), the heat transfer process was similar at several sites where turbulent heat flux was measured directly [*McPhee*, 1992]. Those results raised the possibility of using historical mixed layer temperature and salinity data, along with estimates of surface (ice-ocean) stress, to obtain reliable estimates of F_w.

For more than a year beginning in March 1975 the Arctic Ice Dynamics Joint Experiment (AIDJEX) project maintained a triangular array of manned drift stations in the central Arctic. Despite a lack of direct oceanic flux measurements the AIDJEX ice, ocean, and atmospheric data collected during the summer of 1975 allow us to investigate temporal and spatial variations in F_w during a time when there was significant solar heating of the mixed layer. Data available from AIDJEX are described in section 2 and are used in section 3 to (1) estimate F_w using AIDJEX salinity-temperature-depth (STD) and ice motion data; (2) obtain an independent estimate of F_w from ice ablation measurements; (3) calculate heat storage in the mixed layer; and (4) estimate total shortwave radiation entering the upper ocean, using measured surface radiation and ice concentration derived from deformation of the AIDJEX manned triangle. Results are compared and discussed in section 4.

2. The AIDJEX Data Set

The AIDJEX program produced a wide variety of data on ice movement and deformation, upper ocean salinity and temperature, air and water stress, and the heat and mass budget of the ice cover [see *Pritchard*, 1980]. A prime objective was to determine the relationship between large-scale ice deformation and the external stress field. The experimental array consisted of a central manned station ("Big Bear") surrounded by a triangle of manned camps ("Blue Fox," "Caribou," and "Snow Bird"), each situated about 100 km from Big Bear. Surrounding the manned array was a circle of 16 data buoys with a diameter of about 800 km. This project was deployed in the Central Beaufort Sea in early April 1975. In the following 2 months it drifted west about 200 km, then southeast about 420 km during the summer. The main camp, Big Bear, broke up and was abandoned in early October 1975. The remaining array then drifted slowly westward, covering about 250 km by the end of the project in May 1976. Basic ice, ocean, and atmospheric data were collected at each of the manned camps throughout the experiment.

2.1. Salinity-Temperature-Depth Data

STD data taken at the four stations are described by *Bauer et al.* [1980]. Casts were typically made once per day to a nominal depth of 750 m at the satellite stations and twice per day (with occasional deep casts) at Big Bear. Coverage at the satellite camps was reasonably complete; however, there were sizable gaps in the record from Big Bear from days 211 to 220 and from day 239 on. The data were calibrated against bottle samples collected with each cast.

Bauer et al. [1980] report that mean differences in temperature between the STD data and bottle samples ranged from −0.02 to 0.03 K, depending both on the location and the data recording method (digital or analog). Standard deviations ranged from 0.02 to 0.06 K. For salinity, mean differences ranged from 0.00 to 0.02 parts per thousand, with standard deviations ranging from 0.00 to 0.05. These errors are several times those expected from present-day, well-calibrated equipment and significantly affect our analysis of the departure of upper ocean temperature from freezing, $\delta T = T - T_f(S)$, which is used to estimate both F_w and changes in heat content. The analysis of *Bauer et al.* [1980] suggests nominal errors of 0.03 for both temperature and salinity for any particular cast, implying an uncertainty of about ±0.03 K in δT. For typical surface stress conditions this implies an uncertainty in F_w of about 5 W m^{-2} for each individual cast, based on the error in temperature alone. For each profile the standard deviation of temperature samples in the mixed layer is at least an order of magnitude smaller than the reported errors, thus most of the variability occurs from cast to cast. Under steady, uniform forcing conditions, averaging five mixed layer temperatures would bring the error in heat flux down to about 1 W m^{-2}. In practice, AIDJEX conditions were neither steady nor horizontally uniform. Besides observational errors, several natural phenomena contributed to variability observed in upper ocean temperature and salinity structure. Eddies [*Manley and Hunkins*, 1985; *D'Asaro*, 1988] were a ubiquitous feature in the pycnocline beneath the AIDJEX array as illustrated by the density structure at station Blue Fox (Figure 1). Density is expressed as $\sigma_0 = \rho(S, T, 0) - 1000$ kg m^{-3}, where $\rho(S, T, 0)$ is seawater density at surface (atmospheric) pressure. The compact eddies were predominantly anticyclonic, with density and velocity disturbances centered near 100 m depth. Although their surface or mixed layer expression was typically small, they represent an anomaly from the surrounding ambient water in the upper pycnocline, increasing short-term variability in inte-

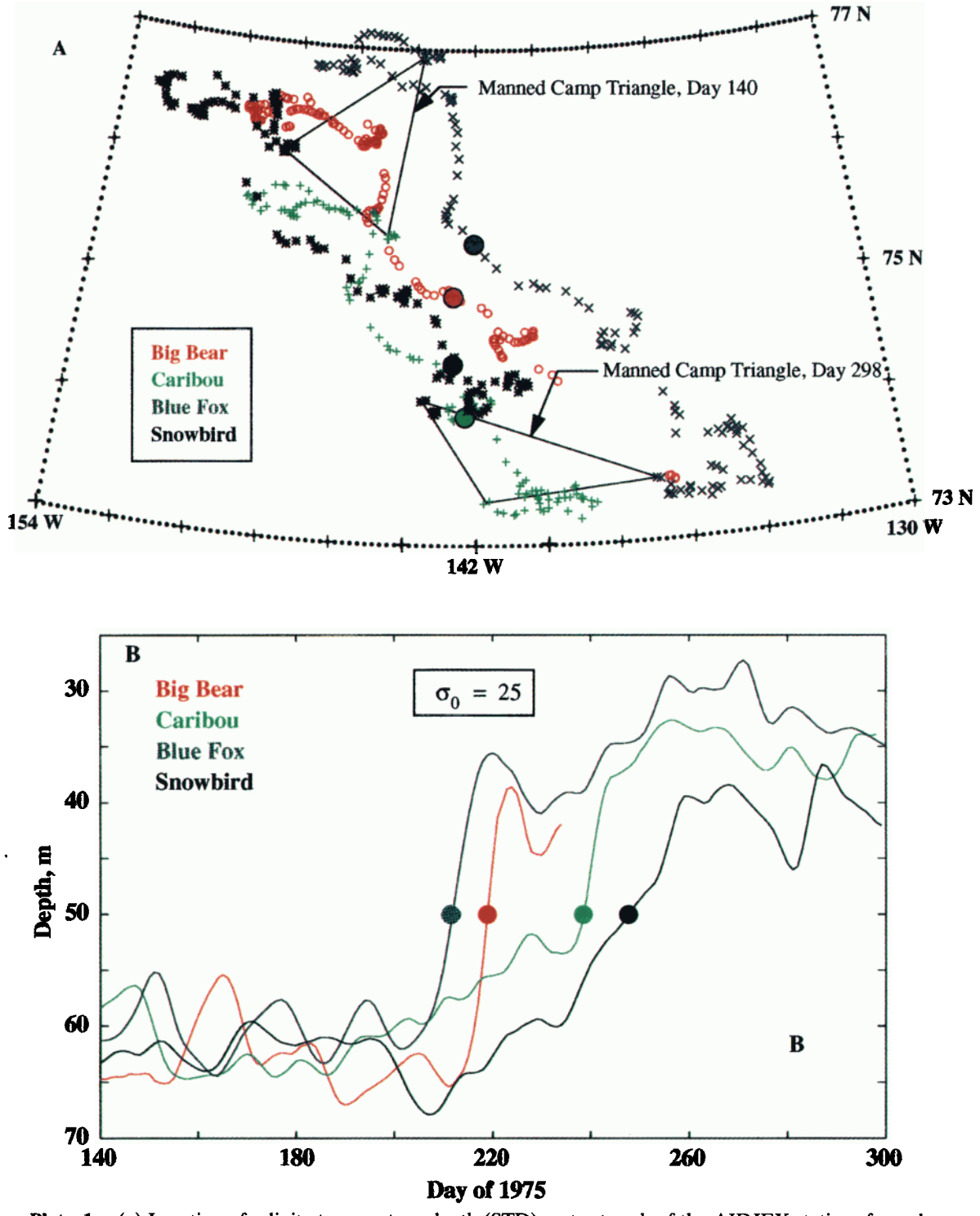

Plate 1. (a) Location of salinity-temperature-depth (STD) casts at each of the AIDJEX stations from days 140 to 300 of 1975. Triangles mark the locations of stations Blue Fox, Caribou, and Snowbird at the start and end of the period. Big Bear was initially centered in the array. (b) Depth of the σ_0 = 25 kg m^{-3} surface, marking the upper limit of the permanent pycnocline. The stations drifted over two distinct, upper ocean density regimes, with the sharp boundary between them marked by the solid color dots in both Plates 1a and 1b.

grated quantities such as upper ocean heat content. We thus disregarded STD casts which were clearly within anticyclonic vortices and interpolated T and S linearly in the "eddy" gaps.

A second important feature in the AIDJEX STD data is that as the camps drifted southeast during the summer, each crossed a region in which the salinity and density in the upper part of the pycnocline increased sharply. Locations of the STD casts at the four manned camps for days 140–300 are shown in Plate 1a. Over the summer the array drifted more than 300 km, with considerable deformation in the outer camp triangle. At

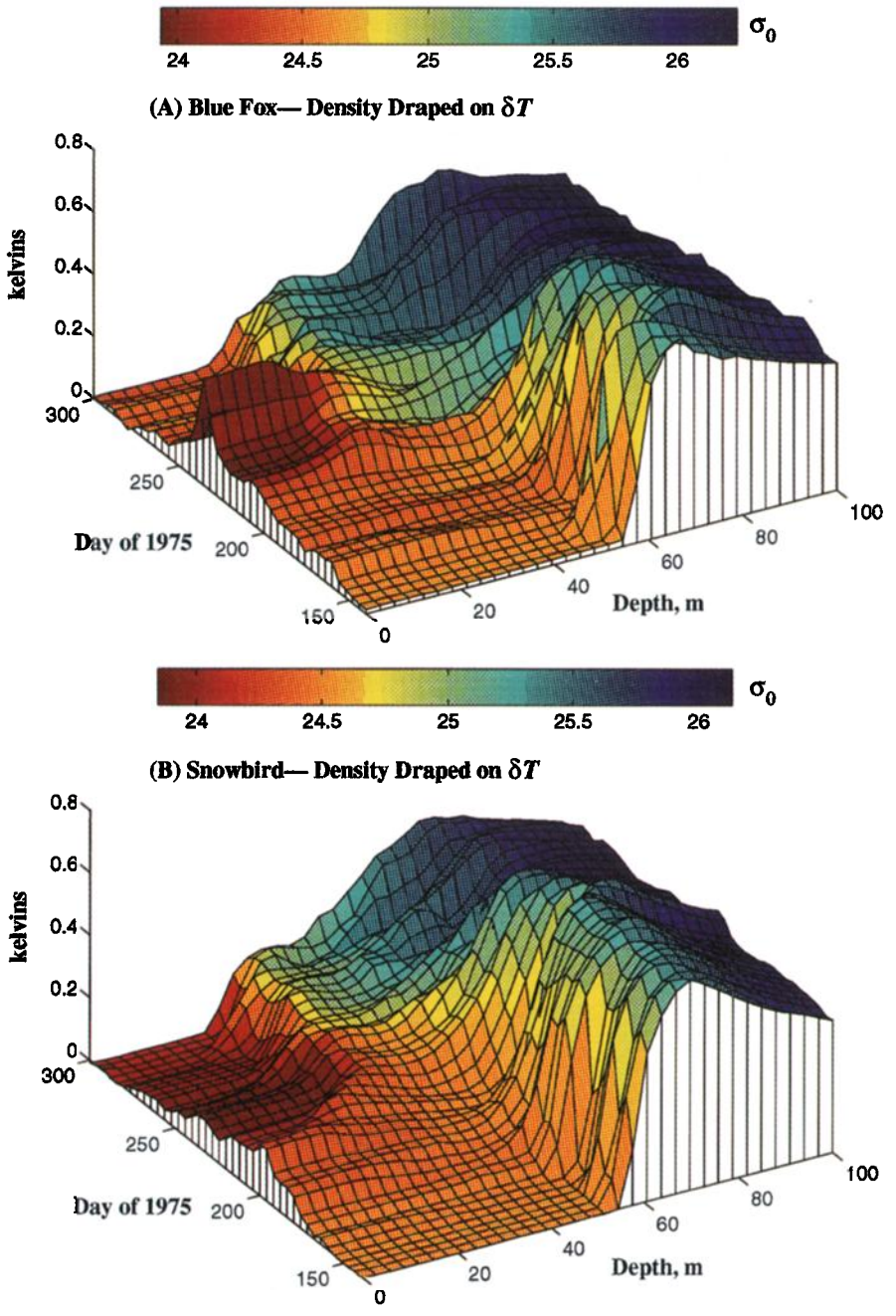

Plate 2. Temperature elevation above freezing (at surface pressure) as the z ordinate, colored by density as functions of time and depth at stations (a) Blue Fox and (b) Snowbird. Density is mainly a function of salinity at low temperatures.

Big Bear, STD casts were available only occasionally after day 239 and ceased entirely when the station was abandoned (day 275). Depth of the σ_0 surface marking the upper limit of the pycnocline is shown for all stations in Plate 1b, after smoothing with a 5-day running mean. While isopycnal elevation often varied by several meters over a period of a few days, it is obvious that each record comprises two different regimes, with the upper part of the pycnocline being more saline in the later part of the period. At each camp a unique transition from one regime to the other may be identified by the time when the σ_0 = 25 kg m^{-3} isopycnal surface rose above 50 m depth. Geographical positions are shown in Plate 1a. The transits span a 40-day period, and all occurred after meltwater had essentially decoupled the upper pycnocline from the surface. Advection of the camps into a differing water mass, rather than local vertical exchange, thus appears to be the dominant factor in modifying the upper pycnocline. Advection across a stationary feature is not the entire story, however. Snowbird crossed into the denser regime on day 247 at a location near to the position occupied by Caribou on day 221. Since Caribou did not make its transit until day 238, the front must have migrated. The general picture afforded by Plate 1a is of a frontal feature aligned roughly north-south along 142°W, tending to move ageostrophically westward. The example illustrates the difficulty of separating horizontal advection from temporal evolution in interpreting upper ocean structure. This is true especially for integral prop-

erties; e.g., mean salinity of the upper 50 m of the water column increased at all the AIDJEX stations over the course of the summer, despite substantial melting.

A more comprehensive view of the upper ocean heat and density structure is provided by perspectives of δT colored by density stratification in the upper 100 m (Plate 2). The $\sigma_0 = 25$ kg m^{-3} surface (Plate 2b), for example, is represented by the transition from yellow to green. At temperatures near freezing, density varies mostly with salinity, so δT and σ_0 are, for practical purposes, independent. Blue Fox and Snowbird are shown since they were the first and last stations, respectively, to cross the front.

Some features of upper ocean heat and density structure are obviously related to the frontal transition; in the 60–80 m layer, for example, heat content is higher prior to crossing (i.e., west of about 143°W). Our main concern here, however, is upper ocean heat flux, and there are some important similarities and differences in the top part of the water column that appear to be unrelated to the position of the front. Until about day 150 the mixed layer at each site was around 50 m deep and near its freezing temperature. For the next 40 or 50 days each warmed slowly but remained relatively well mixed (uniform color). Starting at about day 200 (mid-July), there was a rapid influx of meltwater, largely confined to the upper 20–25 m, which formed a strong seasonal pycnocline (red to yellow gradient). At Blue Fox there was subsequent heating, raising mixed layer temperature above −1.3°C, which was largely absent at Snowbird (and the other camps). As the season progressed, the mixed layer cooled but remained relatively fresh. The plots suggest that heat introduced and thoroughly dispersed through the mixed layer in June and early July was then trapped for the remainder of the summer below the zone of active mixing. One would expect this trapped heat to be regained during fall freeze-up, but mixing at the AIDJEX sites over the following winter and spring (1975–1976) was never strong enough to extract it back to the surface.

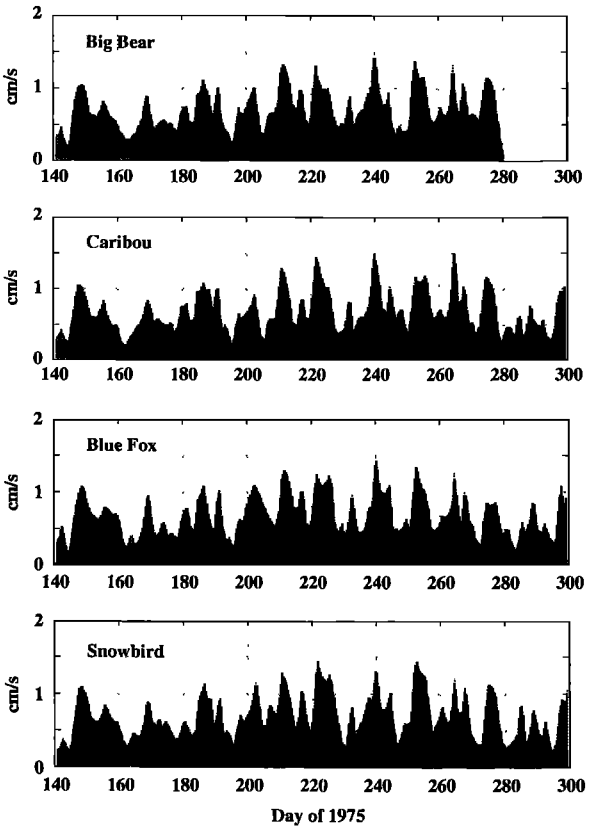

Figure 2. Friction velocity (square root of kinematic stress at the ice-ocean interface) estimated from the ice drift velocity relative to the surface geostrophic current, using a geostrophic drag law for sea ice [*McPhee*, 1979].

2.2. Ice-Ocean Stress

Stress at the ice-ocean interface was estimated using a Rossby similarity law developed from AIDJEX data [*McPhee*, 1979]. The method is as follows. Let $u_{*0} = (\tau_0)^{1/2}$ be the surface friction velocity, where τ_0 is the magnitude of kinematic Reynolds stress at the ice-ocean interface, and $\mathbf{U}_0 = \mathbf{U}_i - \mathbf{U}_g$ be the vector ice velocity relative to surface geostrophic current in the ocean $\mathbf{U}_g$. The magnitude of the friction velocity is obtained from the complex geostrophic drag relation:

$$\frac{|\mathbf{U}_0|}{u_{*0}} = \left| \frac{1}{\kappa} [\log (Ro_*) - A - iB] \right| \qquad (1)$$

where $\kappa = 0.4$ is von Karman's constant, A and B are the Rossby similarity constants, $Ro_* = u_{*0}/fz_0$, is the "surface friction Rossby number," f is the Coriolis parameter, and z_0 is the roughness length for the ice undersurface. Values previously determined to be representative for the AIDJEX stations are $A = 1.91$, $B = 2.12$, and $z_0 = 0.1$ m [*McPhee*, 1979].

The Rossby-similarity drag formulation should not be applied directly to the instantaneous ice velocity when inertial motion is present. The ice cover and underlying mixed layer usually oscillate together so that inertial shear occurs in the upper pycnocline where turbulent transfer is much less efficient. Since stress is proportional to shear between the ice and upper part of the water column, inertial (or tidal) motion causes little stress, unless the ice is constrained by internal forces. For AIDJEX, ice velocity was calculated by differentiating position functions, obtained by fitting satellite navigation records using complex demodulation [*McPhee*, 1988]. The technique partitions ice position records in a moving 24-hour period window into linear plus inertial and tidal components and, when differentiated, provides a running estimate of "mean" velocity. Geostrophic current, which is the current due to sea-surface slope, was estimated from the dynamic topography developed for the AIDJEX model [see *McPhee*, 1979]. The u_{*0} for each of the stations is shown in Figure 2.

A potential source of systematic error in applying (1) comes in specifying the undersurface roughness z_0. The value used here was inferred from the summer free-drift force balance, hence it depends on the 10-m atmospheric drag coefficient, which was taken to be $c_A = 0.0027$, based on integration of pilot balloon profiles [*McPhee*, 1979]. This is larger than the drag coefficient derived from the 25-m meteorological tower profiles. *Leavitt* [1980] suggested $c_A = 0.002$ over the smooth floes on which Big Bear and Caribou were located but considered it to be an underestimate of the average regional drag coefficient. If the lesser value is, in fact, more representative, the typical summer force balance implies a value of $z_0 = 0.03$ m for the ice undersurface and an average reduction in the calculated u_{*0} of about 15%.

2.3. Ice Growth Rates

Wire thickness gauges were set out at each camp to monitor mass changes at the underside of the ice. Thickness changes

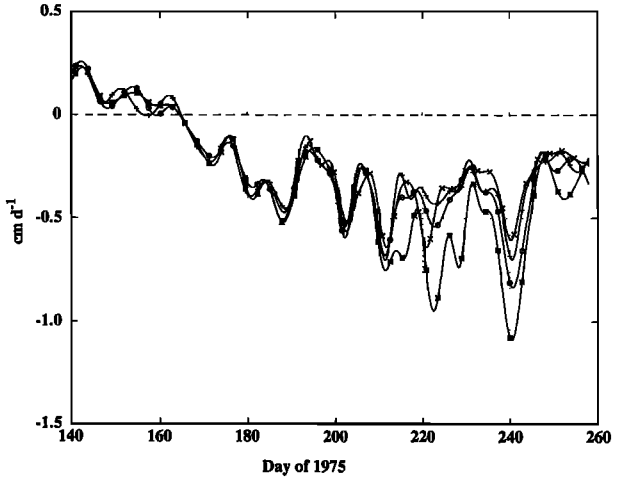

Figure 3. Bottom ablation rates measured at four sites in undeformed, multiyear ice at station Big Bear. Initial ice thicknesses varied between 2.72 and 2.89 m.

were typically measured at 2-day intervals to an accuracy of ±1 mm with respect to reference stakes frozen into the ice at the upper surface. While only two or three gauges were set out at the satellite camps, over a dozen were implanted in the multiyear floe at Big Bear. During the summer melt season an abrupt increase of 0.5–1.0 m in apparent thickness at many of the gauges signaled formation of false bottoms caused by the injection of low-salinity, surface meltwater beneath the ice. The thermodynamics of false bottoms is complex, thus their migration rates alone cannot be used to infer F_w. Only four gauges, all in undeformed ice at Big Bear, provided data unaffected by the freshwater lenses throughout the summer (Figure 3). Bottom melting started about June 15 (day 166) and continued through mid-September, when observations were halted. Cumulative bottom ablation during this period varied between 0.30 and 0.41 m, the average being 0.34 m. Corresponding melt totals at the upper surface varied between 0.22 and 0.34 m, the average being 0.26. This melt pattern differs significantly from earlier drift station data in the central Arctic [e.g., *Untersteiner*, 1961], where observed bottom ablation is generally much less than the surface ablation.

Melt rates at the four sites were similar until early August, when ice at one of the sites (6) began to melt much faster than at the other three. More rapid melting continued at this site throughout the remainder of the summer, resulting in a total bottom ablation that was about 25% larger than the other sites. The variance between melt rates at the other sites also became noticeably larger during August. The reason for these differences cannot be determined with certainty. Although melting and loosening of the reference stakes could have increased errors and contributed to the difference, *Wettlaufer* [1991] also observed significant spatial variability in bottom melting over scales of 0.1 to 100 m, which he ascribed to (1) "shadowing" effects from nearby topographic features such as pressure ridge keels and (2) interfacial instabilities which enhance small-scale ice roughness variations and increase the local F_w. Conditions at the ice-water interface during the summer melt season were conducive to the formation of such instabilities whose evolution during June and July may explain much of the increased variance in August. In the case of site 6 we suspect that some change in the nearby topography or flow direction may have contributed to its anomalous behavior.

2.4. Strain Rates and Ice Concentration

Daily averages of divergence and shear for the manned camp array have been tabulated by *Colony* [1978] and analyzed in detail by *Thorndike and Colony* [1980]. Briefly, the area of the array decreased by about 9% in June, then increased by 5% in July and another 9% in August, then decreased again in September by about 16%. The net divergence experienced by the array during July and August, combined with the disappearance of thinner first-year ice from the leads, should contribute to substantial amounts of open water and solar heat input to the water column during these months. To quantify changes in the amount of open water during the period of interest, we used the ice thickness distribution model of *Thorndike et al.* [1975] and the strain invariants of *Colony* [1978]. Following the development of *Maykut* [1982], we made the following modifications to the original Thorndike et al. treatment: (1) only the thinnest 10% of the ice was allowed to ridge; (2) on average, ice was assumed to ridge to 15 times its original thickness; and (3) the yield curve was replaced by the 30° "teardrop" function proposed by *Rothrock and Hall* [1975]. Since little ridging occurred during the summer, these modifications did not affect thin ice predictions until September and October, when there was substantial convergence and production of young ice in the refreezing leads. Thermal forcing for the ice thickness distribution calculations was similar to that described by *Maykut* [1982], basically utilizing climatological data on incoming longwave radiation from *Marshunova* [1961] and turbulent heat flux data from *Doronin* [1963]. The model was integrated with the above strain and heat balance data to obtain daily estimates of the fractional area of the manned array covered by ice in eight thickness categories, ranging from 0–0.1 m ("open water") to ice thickness over 6.4 m.

Predictions of the area occupied by open water and by 10- to 20-cm thick ice are shown in Figure 4. Ice concentrations during June, July, and August were determined primarily by the observed divergence of the array. Monthly averages of

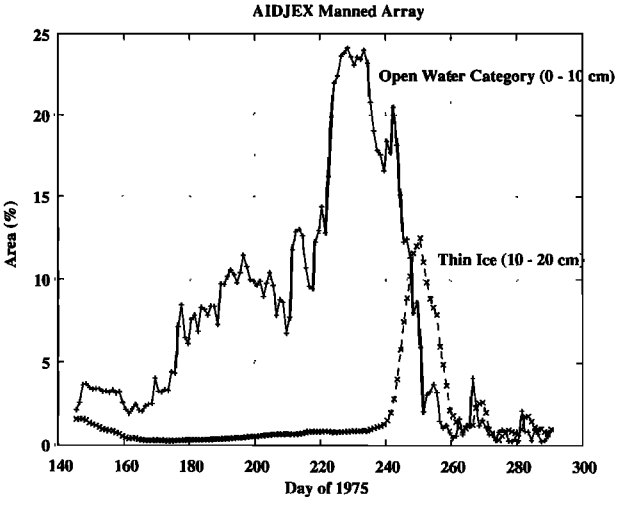

Figure 4. Relative area within the AIDJEX manned array occupied by open water and very thin ice. Estimates were obtained using the thickness distribution model of *Thorndike et al.* [1975] and the strain data of *Colony* [1978].

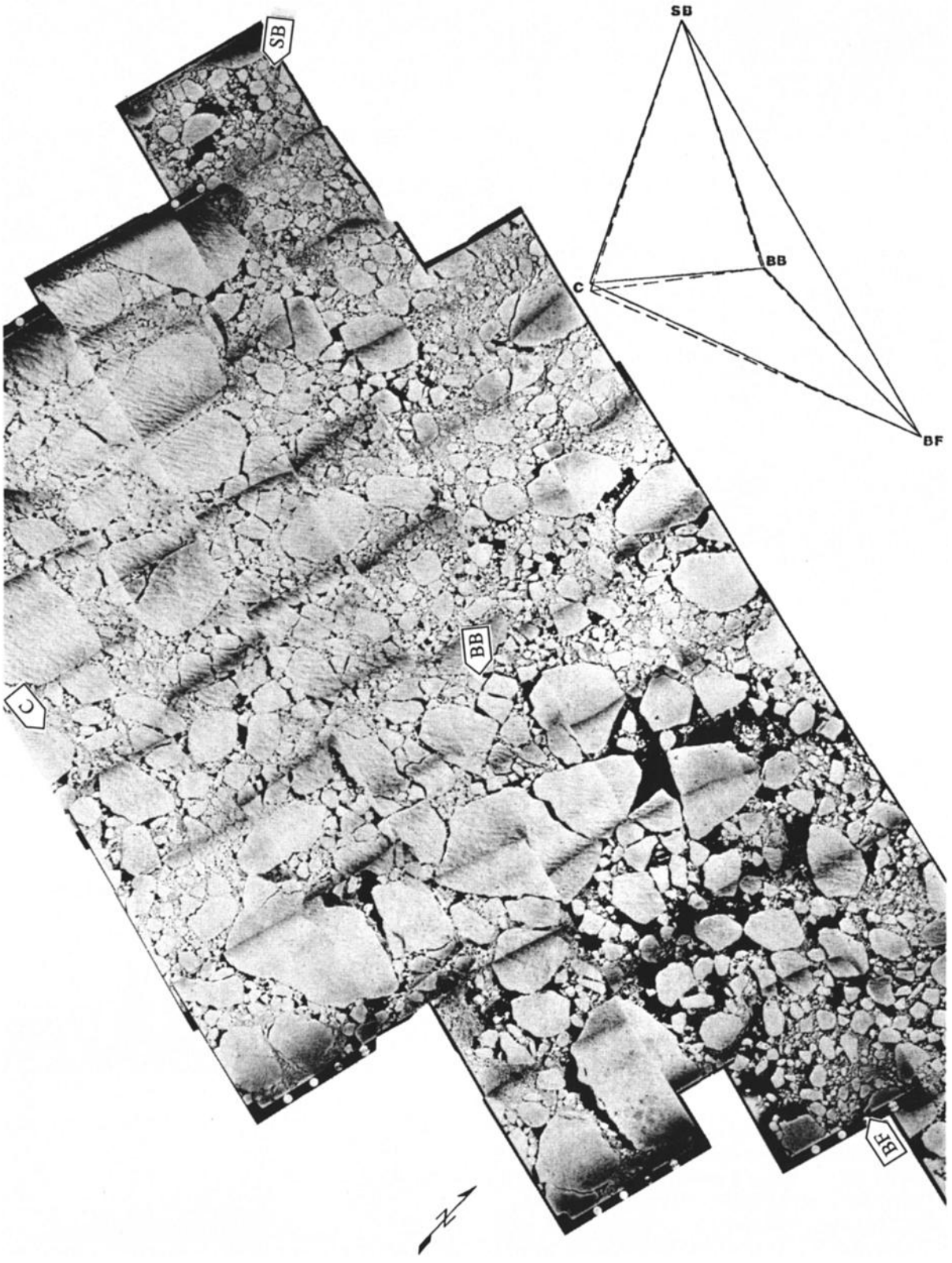

Figure 5. Aerial photographic mosaic of the AIDJEX manned camp triangle taken on August 18, 1975 (day 230), from *Hall* [1978]. Arrows mark the locations of the stations, which are shown schematically using aircraft navigation (dashed lines) and satellite navigation (solid line) by the triangle at top upper right.

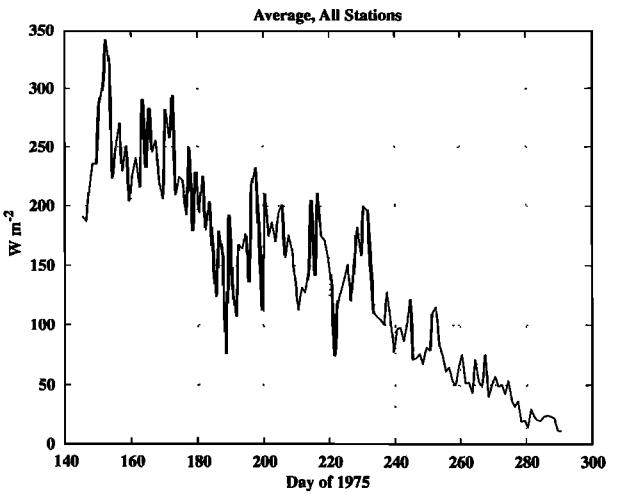

Figure 6. Daily values of incoming shortwave radiation within the AIDJEX array obtained by averaging observations at the four manned camps (drawn from data of *Pautzke and Hornof* [1978]).

open water were 3.6% during June, 9.1% during July, 17.7% during August, 5.7% during September, and 0.6% during October. Maximum open water values occurred during the third week of August, when F_r was 50–60% of early June values. The peak in the amount of 10- to 20-cm ice during the second week of September reflects the freeze-up of open water created during the preceding 3 months. The area covered by 10- to 40-cm ice generally did not exceed 1–2% during the summer, while thicker first-year ice ($40 < H < 160$ cm) accounted for about 10% of the array. These area predictions appear reasonable, with the possible exception of the open water maximum in mid-August. An aerial photographic mosaic made on August 18 (Figure 5) shows large spatial variations in ice concentration across the region. While open water accounted for as much as 25% of the area in eastern parts of the array between Big Bear and Blue Fox, values in the southwestern part were 7% or less; the average for the mosaic as a whole was 12–15% [*Hall*, 1978]. Predicted values at this time are 8–10% larger, reflecting a 13% net divergence in the array between days 220 and 225. It is not known to what degree this mosaic represents conditions either before or after August 18. Although the evidence clearly indicates that there were large amounts of open water present in the region during the second half of August, differences between theory and observation can arise because local deformation is a function not only of the large-scale strain field, but also of small-scale random motions unrelated to that field.

2.5. Shortwave Radiation

Incoming shortwave radiation was measured at all stations. Daily totals for 1975 have been reported by *Pautzke and Hornof* [1978]. Differences between individual stations were usually no more than 10–15%, while monthly totals agreed to within about 5%. Figure 6 shows values averaged over the available stations. Caribou data before day 227 were ignored due to sensor and/or calibration problems, while data from Big Bear were only available through day 269. Monthly totals were 627 MJ m^{-2} for June, 436 MJ m^{-2} for July, 365 MJ m^{-2} for August, and 173 MJ m^{-2} for September. Totals for June and July were 20–25% smaller than climatological averages reported by *Marshunova* [1961], while August was 1% smaller and September 10% larger. The cumulative total during June–September was 1744 MJ m^{-2}, 14% lower than Marshunova's estimate.

3. Results

Data described above provide the basis for examining the relationships among shortwave radiation, summer heating of the mixed layer, and energy exchange at the ice-water interface. F_w was calculated following a simplified scheme, based on direct turbulent heat flux measurements made during three Arctic drift station projects [*McPhee*, 1992]:

$$F_w = \rho c_p c_h u_{*0} \delta T \tag{2}$$

where ρ is water density, c_p ($=3980$ J kg^{-1}) is specific heat for seawater near freezing, and $c_h = 0.006$ is the heat transfer coefficient. Time series of u_{*0} (Figure 2) and δT were combined to obtain F_w for each station (Figure 7). Average temperature and salinity in the 5- to 10-m depth interval were used to determine mixed layer departure from freezing. The heat flux time series comprise mainly a modulation of mixed layer temperature elevation by the local turbulent friction velocity. During summer, u_{*0} varies closely with the wind speed, so we expected a fair amount of short-term variability in F_w as transient pressure systems passed over the camps. Figure 2 shows

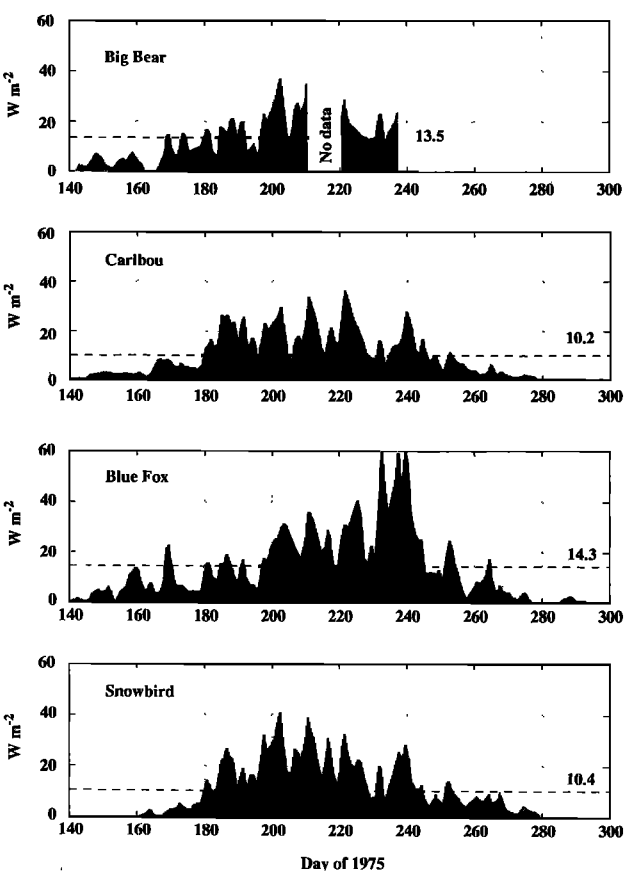

Figure 7. Oceanic heat flux ($F_w = \rho c_p c_h u_{*0} \delta T$) for the AIDJEX manned stations. Gaps in the Big Bear record result from gaps in the salinity-temperature-depth (STD) data. Dashed-line horizons indicate average values for the data shown.

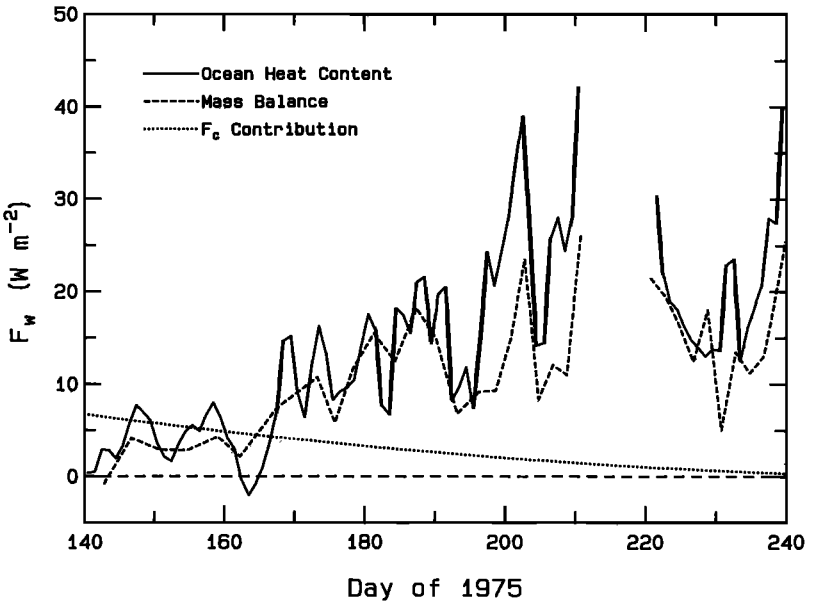

Figure 8. Time-dependent changes in F_w at Big Bear calculated from ocean temperature and velocity measurements (solid curve) compared with values inferred using averaged mass balance data from undeformed ice (dashed curve). The amount of heat contributed by F_w to upward conduction at the ice-water interface F_c was estimated using the model of *Maykut and Untersteiner* [1971] and is shown as the dotted curve.

that response to the wind was relatively uniform across the array; e.g., note the similar values for u_{*0} at all stations during storms centered around days 187 and 240. More surprising, however, were the spatial differences in heat flux under similar stress conditions. During the earlier storm (day 187), heat flux at the western stations, Caribou and Snowbird, was at least 10 W m^{-2} larger than at Big Bear and Blue Fox, and this was rather typical of the spatial variability across the array during the entire summer. Around day 240 the differences became more extreme, with heat flux at Blue Fox larger by more than 30 W m^{-2}. This results directly from the much higher mixed layer temperature at Blue Fox (Plate 2) since turbulent stress was about the same at all camps. After day 300, mixed layers at the three surviving stations remained near freezing for the remainder of the project and heat flux was negligible relative to the summer values.

Errors in the calculation of F_w result from errors in δT and u_{*0}, as described in section 2, and also from uncertainty in c_h, the heat transfer coefficient. Values found from direct flux measurements during MIZEX 84 and the two Coordinated Eastern Arctic Experiment (CEAREX 88 and CEAREX 89) drifts were 0.006, 0.006, and 0.005, respectively [*McPhee*, 1992]. The last was in late winter north of Fram Strait, with generally low heat flux levels and relatively fewer samples. The other two projects took place during mid- or late summer. The numerical value used here, $c_h = 0.006$, was also the value found from flux measurements under multiyear ice during a late summer storm in the western Weddell Sea [*McPhee and Martinson*, 1994]. The most likely source of systematic error in F_w comes from u_{*0}. As discussed above, if wind stress was overestimated in the force balance used to infer z_0, then F_w would also be overestimated approximately in proportion to the square root of the stress. For the smoothing used on the oceanographic parameters, one might expect random errors of order ± 1 W m^{-2} in daily F_w estimates due to uncertainty in δT. The main source for error in season-long mean values for F_w would come from systematic errors in u_{*0} and c_h. Using what we believe are reasonable ranges for these parameters, the combined systematic error is estimated to be approximately 30%.

Heat transported from the water to the ice-ocean interface is balanced by the conductive flux in the ice F_c and latent heat associated with phase changes at the bottom:

$$F_w = F_c - \rho_i L \dot{d} \tag{3}$$

where $\dot{d}$ is the ice growth rate and L is latent heat, adjusted for brine volume. This provides an independent method for obtaining F_w from measurements in the ice [e.g., *Untersteiner*, 1961; *Lake*, 1967; *McPhee and Untersteiner*, 1982]. *Wettlaufer* [1991] examined the method in detail, using data from 11 thickness gauge and ice temperature sites situated on one floe during CEAREX 88. He found large spatial variations (especially during periods of melting) which appeared to be related to local topographic differences. We also saw substantial intersite variability in growth rates (Figure 3), occurring primarily in the later part of the melt season after day 212. To compare the amount of heat received by undeformed ice and the amount released from the water column, we first estimated $\rho_i L\dot{d}$ from average growth rates at Big Bear, assuming brine volume in the ice to be 10%. Ice temperature data were not available, so F_c was calculated theoretically, using the thermodynamic ice growth model of *Maykut and Untersteiner* [1971]. Equation (3) then provides an estimate of F_w that agrees well with independent estimates derived from oceanic parameters at Big Bear (Figure 8), except during the peak heat flux period around day 200. The differences after day 200 appear to be systematic and are unlikely to have resulted from random errors in either the ocean or mass balance. A possible explanation for the difference is discussed in section 4.

Time-dependent changes in upper ocean heat storage were investigated by calculating heat content Q, defined as the energy that would have to be extracted from the water column

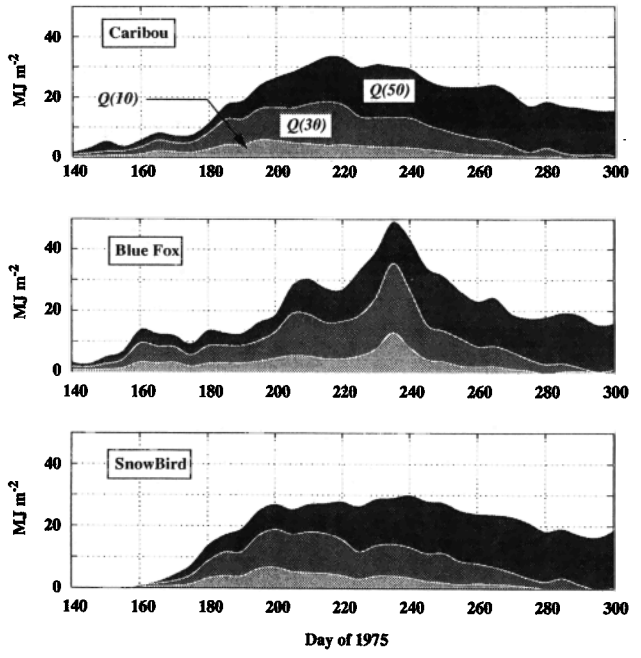

Figure 9. Summer heat content of the water column above three different depths for stations with continuous STD records.

above some reference level z in order to bring it to its freezing temperature (at surface pressure):

$$Q(z) = \int_z^0 \rho c_p \delta T dz' \qquad (4)$$

Q was calculated for the water column above three levels ($z = -10, -30, -50$ m) to illustrate the seasonal development (Figure 9). Early in the summer, there was little heat stored in the upper 50 m, but as the season progressed, Q_{50} reached maximum values between 30 and 50 MJ m^{-2} (equivalent to about 10–18 cm of ice melt), then began to diminish as a result of surface heat loss and decreased shortwave input. By day 300, nearly all of the heat had been extracted from the upper 30 m, however, a significant fraction remained between 30 and 50 m. As discussed in section 2.1, this heat was buffered from the penetration of winter mixing for the remainder of the project, and although the picture was complicated by southeast advection into a water mass with different pycnocline properties, the mixed layer appears to have been a source, rather than a sink, of heat for the upper pycnocline. The tendency would be reinforced by downwelling associated with Ekman convergence in the anticyclonic Beaufort Gyre. It should be noted, however, that one powerful storm, especially during freeze-up when ice is mobile and turbulence is enhanced by haline convection, could have extracted the stored heat and changed the balance.

To estimate the amount of solar heat entering the water, we combined the measured shortwave radiation flux at the upper surface (Figure 6) with the open water estimates obtained from deformation of the manned camp triangle (Figure 4). Figure 10 shows the area-averaged shortwave input at the top of the water column and the amount absorbed below the bottom of the ice (assumed to be at the 3-m level). The difference between these two curves is the amount of energy potentially available for lateral melting on floe edges. However, except in narrow leads, turbulent mixing is likely to redistribute much of this energy beneath the ice where it would contribute to F_w, rather than to lateral melting. Ocean turbulence was relatively intense during most of the summer (Figure 2), thus there was probably strong vertical exchange of heat between the leads and underlying water, leaving little energy available for lateral melting. Heat input to the water column during July increased gradually by about 5 W m^{-2} due to decreasing ice concentration. Strong divergence and increased open water caused the heat input to more than double during the first half of August. The result of this heating can be seen in the increased F_w values at all stations during the second half of August.

Cumulative energy fluxes to and from the water column are graphed in Plate 3. Total solar input to the water over the summer is estimated to be 150 MJ m^{-2}, which includes a contribution of about 18 MJ m^{-2} from energy transmission through ice in the 10- to 180-cm categories. Energy transmission through multiyear and pond-covered ice is uncertain and was not included in this estimate. Total heat lost from the water column at Blue Fox exceeded that at Snowbird and Caribou by more than 50 MJ m^{-2}, enough to melt an additional 20 cm of ice. Disregarding Blue Fox, the agreement between our estimates of heat gained by the mixed layer with that lost or stored is surprisingly close. At Caribou, for example, the total upward heat loss (140 MJ m^{-2}) plus the 15 MJ m^{-2} stored in the upper 50 at the end of the summer (see Figure 9) is within about 3% of the estimated radiative heating. This also indicates that little energy was available for lateral melting. The heat received by undeformed ice at Big Bear totaled about 110 MJ m^{-2}. Taking into account the 30 MJ m^{-2} remaining in the water column, there is only a difference of about 7 MJ m^{-2} between average energy input to the water and the heat input to level ice. Interpretation of these results is, of course, complicated by advective changes unrelated to local energy input and by uncertainties in the calculation of ice concentration and F_w.

4. Discussion

Our primary objective has been to demonstrate that the oceanic heat flux to the ice in the central Arctic is derived

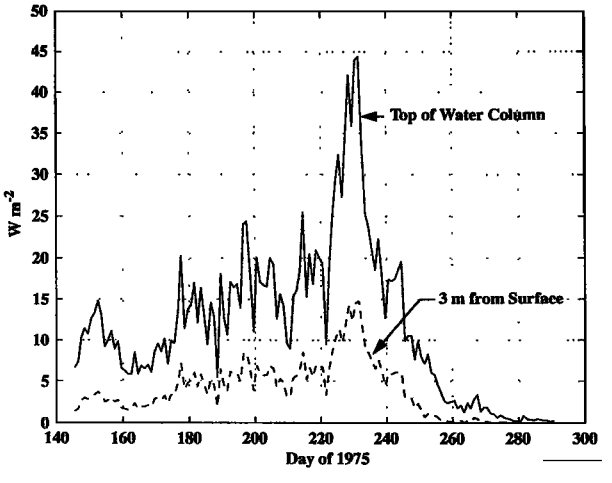

Figure 10. Estimated input of shortwave radiation to the ocean through leads. The dashed curve shows the amount of energy absorbed below the 3-m level in clear Arctic water according to spectral extinction coefficients used by *Perovich* [1983].

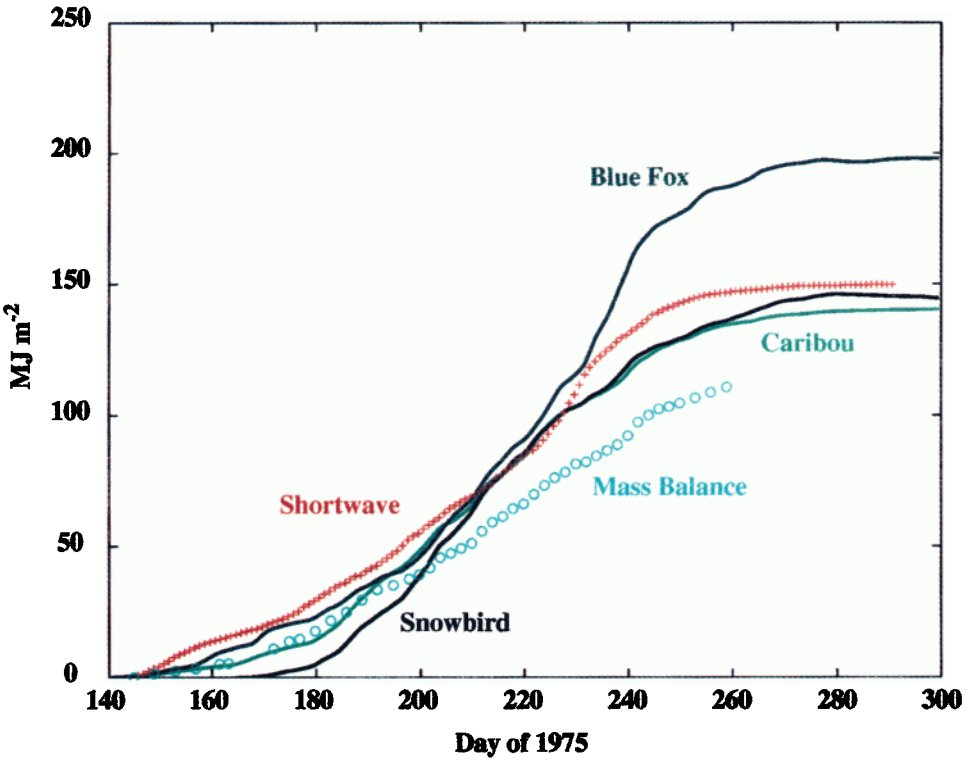

Plate 3. Cumulative energy transfers showing (1) solar heat input to the top of the water column beneath leads and first-year ice (pluses); (2) heat losses from the water to the ice at Blue Fox, Caribou, and Snowbird (solid curves), and (3) heat received from the water by undeformed ice at Big Bear (circles).

mainly from shortwave radiation that enters the mixed layer through the ice cover. Reexamination of the AIDJEX data set convincingly supports this view. Not only are there strong seasonal signals in upper ocean heat content (Figure 9) and F_w (Figure 7), but also the magnitude and temporal change in these quantities are in reasonable agreement with our best estimate of solar heat input to the water (Figure 10 and Plate 3). The large variability in heat flux observed across the manned camp array also suggests a surface source for the heat: day 220 marked the beginning of several days of strong divergence, open water production (Figure 4), and increased insolation to the mixed layer (Figure 10). Mixed layer temperature rose dramatically at Blue Fox but not at Caribou and Snowbird. Examination of the photomosaic taken on day 230 (Figure 5) shows that opening indicated by the strain field was not uniform across the region but was concentrated, instead, between Big Bear and Blue Fox. The rate of solar heat input to the mixed layer in this area was substantially greater than the rate at which the water could lose the absorbed heat to the ice through F_w, thus the mixed layer warmed.

Assuming that ocean heat flux is negligible during winter, the summer values of F_w at Caribou, Blue Fox, and Snowbird imply an annual mean heat loss from the ocean to the ice of 5.1 W m^{-2}, while the mass balance data from Big Bear suggest a value closer to 3.5 W m^{-2}. The difference between the ocean and mass balance estimates may represent additional heat expended in more rapid melting of deformed ice. Our method for determining F_w from oceanic parameters is geared to a regional average since it depends on mixed layer temperature and friction velocity derived from the summer force balance. While δT will not change much across a typical floe, we do expect large variation in turbulent stress beneath heterogeneous, multiyear ice. More vigorous turbulence under rougher ice will enhance turbulent heat flux locally. The thickness distribution calculations indicate that undeformed, multiyear ice made up 35–50% of the summer ice pack, deformed ice 30–35%, with first-year ice and open water accounting for the rest. Assuming that F_w values were comparable beneath first-year and undeformed multiyear ice, then the rate of heat transport to the deformed ice would be about twice that to the level ice.

Plate 3 shows that heat extracted from the ocean over a melt season may vary by as much 35% as determined at points separated by only 100–200 km. The main source of this variability is the amount of opening dictated by dynamic activity of the ice as it responds to passing weather systems, rather than any underlying regional differences in the heat content of the ocean in or below the main pycnocline (Plate 2 illustrates this; heat from the layer 60 to 80 m deep would have to pass through the temperature minimum at around 45 m to reach the ice). In general terms, we find good agreement between our estimates of solar heat input to the ocean, based on deformation of the AIDJEX manned camp array, and upward oceanic heat flux, especially at stations Snowbird and Caribou. However, we are unable to directly account for a significant fraction of the ocean heating. At Blue Fox, F_w plus Q_{50} totaled about 215 MJ m^{-2} by the end of the summer. This is 65 MJ m^{-2} more than our calculations indicate. At Snowbird and Caribou, on the other hand, Figures 5 and 9 suggest that we are likely to have overestimated shortwave input during August. Our calculations also fail to account for lateral melting on floe edges, which acts as a sink for shortwave energy absorbed in the leads. At Big

Bear, lateral melting and erosion totaled as much as 10 m [*Maykut and Perovich*, 1987].

A source of additional energy not treated here is associated with melt ponds which cover 20–50% of the surface of multiyear ice and an even larger percentage of flatter, first-year ice. These ponds transmit a much greater fraction of F_r to the ocean than does the surrounding bare ice [*Grenfell and Maykut*, 1977]. This is due not only to lower albedos and smaller ice thickness beneath the ponds, but also to reduced scattering and absorption in the underlying ice. Unfortunately, we lack sufficient information about temporal changes in their depth, optical properties, and areal coverage to make a reliable estimate of their contribution to mixed layer heating. Ignoring the extra energy entering the ocean beneath these ponds causes us to overestimate the amount of heat that must be mixed downward from the leads to explain observed mixed layer temperatures. This, in turn, affects predictions of lateral melting and ice concentration. While the amount of energy involved is unknown at this point, it is certainly much less than the deficit noted at Blue Fox.

The greatest uncertainty in our analysis is related to the effects of lateral advection. Sea ice is quite mobile relative to the underlying water, and because of Ekman dynamics, its motion is mostly transverse to the bulk of the mixed layer. Since a sizable part of the solar energy input to the mixed layer is not transferred immediately to the ice, stored heat will move relative to the ice cover that existed when it was absorbed. This means that the integrated history of upper ocean warming observed at a particular location does not necessarily reflect the local strain history of the ice. In the case of the AIDJEX array we suspect that the initial westward displacement near the time of summer solstice produced substantial opening somewhere between the array and Banks Island. Significant opening was not observed locally (Figure 10), but we believe that it was more pronounced to the east of Blue Fox and that its effects can be seen when the ice moved back toward the east. This is shown most clearly by the "plateaus" in δT centered around 45 m depth in Plate 2. In the AIDJEX case, much of this heat introduced early in the melt season was then "trapped" by rapid influx of meltwater starting at about day 200 and was still present toward the end of the following winter. Bottom ablation at AIDJEX averaged 34 cm. Earlier observations at Station Alpha showed 22- and 24-cm summer ablation during 1957 and 1958, respectively [*Untersteiner*, 1961], and 10 cm at Station Alpha II in 1959 [*Hanson*, 1965]. Both drifts were farther north than AIDJEX, suggesting that typical summer heat flux is smaller in the interior of the basin, especially where drift tends toward convergence. Because F_w is so closely related to ice concentration, deformation fields monitored by synthetic aperture radar satellites may prove useful for estimating its spatial variation within the Arctic Basin.

Our results emphasize the importance of the thickness distribution of sea ice, especially in the thinner categories, for determining the oceanic heat flux. Of particular concern is the area covered by ice less than a meter in thickness at the onset of summer melting. Its destruction accounts for most of the open water produced during the first part of the melt season. This is well illustrated by the behavior of the AIDJEX array, which underwent a net convergence of about 4% during June and July, yet contained nearly 8% open water at the beginning of August. Melt ponds, which may significantly enhance shortwave input to the water, were not considered in this study, and their role in the regional heat and mass balance remains to be determined.

Although we had hoped to obtain some estimate of how absorbed shortwave energy was partitioned between F_w and lateral melting on floe edges, this was not possible due to uncertainties caused by melt ponds and advection. We note that one subtlety of advection is that it works to reduce the positive feedback between lateral melting and insolation. The capacity of the mixed layer to store heat means that if an area of low concentration ice moves relative to the upper ocean, heat which might otherwise go to edge melting gets left behind, distributed in the mixed layer. Consequently, the tendency for edge melting to rapidly increase open water area is reduced, perhaps substantially. Research on the general topic of how solar heating is absorbed and distributed in and under leads, melt ponds, and thin ice should receive high priority in future field programs that address the surface heat and mass budget.

The STD data show that the summer mixed layer is horizontally inhomogeneous, with substantial variations in temperature and heat content which presumably reflect corresponding variations in ice concentration and solar heating. By impeding the exchange of energy between the ocean and the ice, the molecular sublayers near the ice-water interface allow the polar mixed layer to store heat for weeks to months as indicated by significant departures of mixed layer temperature from freezing. This provides a very useful tool for monitoring oceanic heat flux using buoy-derived drift rates and mixed layer temperature and salinity. It should be noted, however, that local mixed layer temperature does not necessarily reflect the strain (opening and closing) history of the ice on which a buoy or station is deployed.

Despite the uncertainties the picture which emerges from this study is reasonably consistent and quantitatively plausible. It differs, however, from the view usually taken in large-scale models of the ice-ocean system. Instead of being a small flux (2–3 W m^{-2}) that remains relatively constant throughout the year, F_w is strongly seasonal in nature, locally reaching values that can exceed 40–60 W m^{-2}. Since the ice pack and mixed layer move differentially, F_w represents an important term in the heat budget which is not necessarily tied to the purely local deformation or insolation history. While it is not clear how a more sophisticated treatment of F_w in ice models will affect predictions of the thermodynamic equilibrium thickness, it seems likely that tying the oceanic heat flux more realistically to divergence and open water production and to oceanic heat storage during the summer may lead to better understanding of both regional differences and interannual variability in the polar ice packs.

Acknowledgments. We are indebted to Tom Manley for furnishing the AIDJEX STD and navigation data in digital form. This work was supported by the National Science Foundation under grants DPP-9113981 (G.A.M.) and DPP-9210134 (M.G.M.) and by the Office of Naval Research under grant N00014-90-J-1075 (G.A.M.) and contract N00014-94-C-0023 (M.G.M.).

References

Aagaard, K., L. K. Coachman, and E. C. Carmack, On the halocline of the Arctic Ocean, *Deep Sea Res., Part A*, *28*, 529–545, 1981.

Bauer, E., K. Hunkins, T. O. Manley, and W. Tiemann, Arctic Ice Dynamics Joint Experiment 1975–1976, Physical Oceanography Data Report, Salinity, Temperature and Depth Data, vols. 1–4,

Tech. Rep. 8-11, CU-8-80–CU-11-80, Lamont-Doherty Geol. Obs., Columbia Univ., Palisades, N. Y., 1980.

Coachman, L. K., and C. A. Barnes, The contribution of Bering Sea water to the Arctic Ocean, *Arctic*, *14*, 147–161, 1962.

Colony, R., Daily rate of strain of the AIDJEX manned triangle, *AIDJEX Bull. 39*, pp. 85–110, Div. of Mar. Resour., Univ. of Wash., Seattle, 1978.

Crary, A. P., Arctic ice island and shelf ice studies, in *Scientific Studies at Fletcher's Ice Island, T3, 1952–1955*, vol. 3, pp. 1–37, *Geophys. Res. Pap. 63*, Air Force Cambridge Res. Cent., Bedford, Mass., 1960.

D'Asaro, E. A., Observations of small eddies in the Beaufort Sea, *J. Geophys. Res.*, *93*, 6669–6684, 1988.

Doronin, Y. P., On the heat balance of the Central Arctic (in Russian), *Proc. Arctic Antarctic Res. Inst.*, *253*, 178–184, 1963.

Grenfell, T. C., and G. A. Maykut, The optical properties of ice and snow in the Arctic Basin, *J. Glaciol.*, *18*, 445–463, 1977.

Hall, R. T., Seasonal photo mosaics of the AIDJEX triangle, *AIDJEX Bull. 39*, pp. 79–84, Div. of Mar. Resour., Univ. of Wash., Seattle, 1978.

Hanson, A. M., Studies of the mass budget of arctic pack ice floes, *J. Glaciol.*, *5*, 701–709, 1965.

Josberger, E. G., Sea ice melting in the marginal ice zone, *J. Geophys. Res.*, *88*, 2841–2844, 1983.

Lake, R. A., Heat exchange between water and ice in the Arctic Ocean, *Arch. Meteorol. Geophys. Bioklimatol., Ser. A*, *16*, 242–259, 1967.

Leavitt, E., Surface-based air stress measurements made during AIDJEX, in *Sea Ice Processes and Models*, edited by R. Pritchard, pp. 419–429, Univ. of Wash. Press, Seattle, 1980.

Manley, T. O., and K. L. Hunkins, Mesoscale eddies of the Arctic Ocean, *J. Geophys. Res.*, *90*, 4911–4930, 1985.

Marshunova, M. S., Principal characteristics of the radiation balance of the underlying surface and of the atmosphere in the Arctic (in Russian), *Proc. Arctic Antarctic Res. Inst.*, *229*, 5–53, 1961.

Maykut, G. A., Large-scale heat exchange and ice production in the central Arctic, *J. Geophys. Res.*, *87*, 7971–7985, 1982.

Maykut, G. A., The surface heat and mass budget, in *The Geophysics of Sea Ice*, edited by N. Untersteiner, pp. 395–463, Plenum, New York, 1986.

Maykut, G. A., and D. K. Perovich, The role of shortwave radiation in the summer decay of a sea ice cover, *J. Geophys. Res.*, *92*, 7032–7044, 1987.

Maykut, G. A., and N. Untersteiner, Some results from a time-dependent thermodynamic model of sea ice, *J. Geophys. Res.*, *76*, 1550–1575, 1971.

McPhee, M. G., The effect of the oceanic boundary layer on the mean drift of sea ice: Application of a simple model, *J. Phys. Oceanogr.*, *9*, 388–400, 1979.

McPhee, M. G., The upper ocean, in *The Geophysics of Sea Ice*, edited N. Untersteiner, pp. 339–394, Plenum, New York, 1986.

McPhee, M. G., Analysis and prediction of short term ice drift, *Trans. ASME, J. Offshore Mech. Arctic Eng.*, *110*, 94–100, 1988.

McPhee, M. G., Turbulent heat flux in the upper ocean under sea ice, *J. Geophys. Res.*, *97*, 5365–5379, 1992.

McPhee, M. G., and D. G. Martinson, Turbulent mixing under drifting pack ice in the Weddell Sea, *Science*, *263*, 218–221, 1994.

McPhee, M. G., and N. Untersteiner, Using sea ice to measure vertical heat flux in the ocean, *J. Geophys. Res.*, *87*, 2071–2074, 1982.

McPhee, M. G., G. A. Maykut, and J. H. Morison, Dynamics and thermodynamics of the ice/upper ocean system in the marginal ice zone of the Greenland Sea, *J. Geophys. Res.*, *92*, 7017–7031, 1987.

Mellor, G. L., M. G. McPhee, and M. Steele, Ice-seawater turbulent boundary layer interaction with melting or freezing, *J. Phys. Oceanogr.*, *16*, 1829–1846, 1986.

Panov, V. V., and A. O. Shpaikher, Influence of Atlantic waters on some features of the hydrology of the Arctic Basin and adjacent seas, *Deep Sea Res.*, *11*, 275–285, 1964.

Pautzke, C. G., and G. F. Hornof, Radiation program during AIDJEX: A data report, *AIDJEX Bull. 39*, pp. 165–185, Div. of Mar. Resour., Univ. of Wash., Seattle, 1978.

Perovich, D. K., On the summer decay of a sea ice cover, Ph.D. dissertation, 176 pp., Geophys. Program, Univ. of Wash., Seattle, 1983.

Perovich, D. K., and G. A. Maykut, Solar heating of a stratified ocean in the presence of a static ice cover, *J. Geophys. Res.*, *95*, 18,233–18,245, 1990.

Pritchard, R. S., (Ed.), *Sea Ice Processes and Models*, 474 pp., Univ. of Wash. Press, Seattle, 1980.

Røed, L. P., A thermodynamic coupled ice-ocean model of the marginal ice zone, *J. Phys. Oceanogr.*, *14*, 1921–1929, 1984.

Rothrock, D. A., and R. T. Hall, Testing the redistribution of sea ice thickness from ERTS photographs, *AIDJEX Bull. 29*, pp. 1–20, Div. of Mar. Resour., Univ. of Wash., Seattle, 1975.

Thorndike, A. S., and R. Colony, Large-scale ice motion in the Beaufort Sea during AIDJEX, April 1975–April 1976, in *Sea Ice Processes and Models*, edited by R. S. Pritchard, pp. 249–260, Univ. of Wash., Seattle, 1980.

Thorndike, A. S., D. A. Rothrock, G. A. Maykut, and R. Colony, The thickness distribution of sea ice, *J. Geophys. Res.*, *80*, 4501–4513, 1975.

Untersteiner, N., On the mass and heat budget of Arctic sea ice, *Arch. Meteorol. Geophys. Bioklimatol., Ser. A*, *12*, 151–182, 1961.

Wettlaufer, J. S., Heat flux at the ice-ocean interface, *J. Geophys. Res.*, *96*, 7215–7236, 1991.

Yaglom, A. M., and B. A. Kader, Heat and mass transfer between a rough wall and turbulent flow at high Reynolds and Peclet numbers, *J. Fluid Mech.*, *62*, 601–623, 1974.

G. A. Maykut, Department of Atmospheric Sciences, University of Washington, Seattle, WA 98195.

M. G. McPhee (corresponding author), McPhee Research Company, 450 Clover Springs Road, Naches, WA 98937 (e-mail:miles@apl.washington.edu)

(Received December 28, 1994; revised June 1, 1995;
accepted June 6, 1995.)